



INSTITUT DE FRANCE
Académie des sciences

Comptes Rendus

Chimie

Dominique Bazin, Marion Rabant, Jérémie Mathurin, Margaux Petay, Ariane Deniset-Besseau, Alexandre Dazzi, Yangyang Su, Etienne P. Hessou, Frederik Tielens, Ferenc Borondics, Marine Livrozet, Elise Boudierlique, Jean-Philippe Haymann, Emmanuel Letavernier, Vincent Frochot and Michel Daudon

Cystinuria and cystinosis are usually related to L-cystine: is this really the case for cystinosis? A physicochemical investigation at micrometre and nanometre scale


Volume 25, Special Issue S1 (2022), p. 489-502

Published online: 30 November 2021

<https://doi.org/10.5802/crchim.135>

Part of Special Issue: Microcrystalline pathologies: Clinical issues and nanochemistry

Guest editors: Dominique Bazin (Université Paris-Saclay, CNRS, ICP, France), Michel Daudon, Vincent Frochot, Emmanuel Letavernier and Jean-Philippe Haymann (Sorbonne Université, INSERM, AP-HP, Hôpital Tenon, France)

 This article is licensed under the
CREATIVE COMMONS ATTRIBUTION 4.0 INTERNATIONAL LICENSE.
<http://creativecommons.org/licenses/by/4.0/>



Les Comptes Rendus. Chimie sont membres du
Centre Mersenne pour l'édition scientifique ouverte
www.centre-mersenne.org
e-ISSN : 1878-1543



Microcrystalline pathologies: Clinical issues and nanochemistry / *Pathologies microcristallines : questions cliniques et nanochimie*

Cystinuria and cystinosis are usually related to L-cystine: is this really the case for cystinosis? A physicochemical investigation at micrometre and nanometre scale

Dominique Bazin^{*,a}, Marion Rabant^b, Jérémie Mathurin^a, Margaux Petay^a, Ariane Deniset-Besseau^a, Alexandre Dazzi^a, Yangyang Su^c, Etienne P. Hessou^c, Frederik Tielens^c, Ferenc Borondics^d, Marine Livrozet^{e,f}, Elise Boudierlique^{e,f}, Jean-Philippe Haymann^{e,f}, Emmanuel Letavernier^{e,f}, Vincent Frochot^{e,f} and Michel Daudon^{e,f}

^a Institut de Chimie Physique, Université Paris-Saclay, 310, rue Michel Magat, 91400, Orsay, France

^b Pathology Department, Necker-Enfants Malades Hospital, 75015 Paris, France

^c General Chemistry (ALGC) – Materials Modelling Group, Vrije Universiteit Brussel (Free University Brussels-VUB), Pleinlaan 2, 1050 Brussel, Belgium

^d Synchrotron SOLEIL, L'Orme des Merisiers, Saint-Aubin, BP 48, 91192 Gif-sur-Yvette Cedex, France

^e INSERM, UMRS 1155, UPMC, Hôpital Tenon, 75970 Paris, France

^f Service d'Explorations Fonctionnelles, Hôpital Tenon, AP-HP, 4, rue de la Chine, 75970 Paris Cedex 20, France

E-mails: Dominique.bazin@u-psud.fr (D. Bazin), marion.rabant@aphp.fr (M. Rabant), jeremie.mathurin@u-psud.fr (J. Mathurin), margaux.petay@universite-paris-saclay.fr (M. Petay), ariane.deniset@u-psud.fr (A. Deniset-Besseau), alexandre.dazzi@u-psud.fr (A. Dazzi), Yangyang.Su@vub.be (Y. Su), Etienne.Paul.Hessou@vub.be (E. P. Hessou), frederik.tielens@vub.be (F. Tielens), ferenc.borondics@synchrotron-soleil.fr (F. Borondics), marine.livrozet@aphp.fr (M. Livrozet), Eliseboud@aol.com (E. Boudierlique), jean-philippe.haymann@tnn.aphp.fr (J.-P. Haymann), Emmanuel.letavernier@aphp.fr (E. Letavernier), vincent.frochot@aphp.fr (V. Frochot), daudonmichel24@gmail.com (M. Daudon)

Abstract. Medical literature indicates clearly that cystinuria and cystinosis, two severe genetic pathologies, are related to the presence of abnormal L-cystine deposits. While L-cystine adopts a hexagonal crystal morphology consistent with its crystallographic structure (hexagonal, P6₁22 space

* Corresponding author.

group), abnormal deposits related to cystinosis display a rectangular shape. Because this is unexpected from the hexagonal crystallographic structure of L-cystine, we have investigated this inconsistency using SEM (scanning electron microscopy) and IR (infrared) spectroscopy at micrometre and nanometre scales. Our data clearly indicate the presence of both L-cysteine and L-cystine. Considering that L-cysteine crystals display a rectangular shape, and that a transition phase between L-cysteine and L-cystine is well known, we propose the following model for deposit evolution in cystinosis. The initial abnormal deposit consists of L-cysteine, with a rectangular crystal morphology. The micrometre scale rectangular crystallite shape is retained after the phase transition equilibrium between L-cysteine and L-cystine is established, with some crystalline L-cysteine still remaining.

Keywords. Cystinuria, Cystinosis, FTIR, SEM, AFM-IR, OPTIR.

Published online: 30 November 2021

1. Introduction

Several genetic pathologies lead to the formation of abnormal deposits in the human body [1–4]. Some induce kidney stone formation and/or crystalline nephropathy [5,6] such as primary hyperoxaluria [7–10], adenine phosphoribosyltransferase deficiency [11–15] or distal renal tubular acidosis [16]. In the case of cystinuria and cystinosis, a precise determination of the chemical composition of the abnormal deposits can be a considerable aid to diagnosis.

Cystinuria is an autosomal recessive disorder arising from a mutation in renal epithelial cell transporters [17–21], which induces a significant reduction in dibasic amino acids and L-cystine (cystine— $C_6H_{12}N_2O_4S_2$) reabsorption by the proximal tubule. The poor solubility of cystine in urine leads to a high risk of cystine precipitation and the formation of cystine crystallites (Figure 1a), and eventually of kidney stones (Figure 1b) [22–25].

Cystinosis [26] is a rare autosomal recessive lysosomal storage disorder, the treatment of which has advanced in recent years [27]. In cystinosis patients, cystine accumulates in the lysosomes of cells [28]. The presence of cystine has been reported in many organs and tissues namely kidneys, eyes, muscles, thyroid and pancreas [29]. A small number of publications have reported physicochemical investigation of abnormal deposits in these tissues. Frazier and Wong [30] have characterised the rectangular extracellular crystalline forms observed in ocular tissue in two childhood and two adult cases by X-ray diffraction (XRD), leading to the identification of cystine crystals. More recently, Centeno *et al.* [31] have confirmed this chemical composition based on Raman spectroscopy analysis of abnormal deposits present in liver and spleen. Note that various extracellular matrices and proteins may affect the initial crystal structure.

Based on our previous investigation on kidney stones composed of cystine [24], such results are quite surprising. The crystallographic structure of cystine reported by Dahaoui *et al.* [32], displays the space group $P6_122$, predicting that cystine crystallites should exhibit hexagonal morphology in kidney stones; however in cystinosis cases cystine crystallites with a rectangular morphology are observed.

This unusual cystine crystal habit in cystinosis pathology requires investigation using a panel of physicochemical analytical tools able to decipher their morphology and chemistry at the micrometre and then the nanometre scale [33–38]. To do this, we undertook a structural and spectroscopic analysis of such abnormal deposits using scanning electron microscopy (SEM) [14,39,40], μ FTIR (Fourier Transform InfraRed) [14,41,42], AFM-IR (atomic force microscopy coupled with IR) spectroscopy [43,44] and OPTIR (Optical Photothermal IR) spectroscopy [45,46].

SEM offers the opportunity to directly observe the morphology and size of crystallites at the micrometre scale and contributes significantly to the structural description of cystine crystals (see for examples [47–54]). μ FTIR spectroscopy constitutes the gold standard for precisely determining the chemical composition of kidney stones [41,42,55,56]. AFM-IR [43,44] and OPTIR [45,46] are able to collect IR spectra beyond the diffraction limit i.e. around 50 nm and 500 nm, respectively. The complete set of techniques can precisely describe the morphology and chemical nature of the abnormal deposits in tissues or cells in cystinuria and cystinosis at the submicrometre scale.

2. Materials and methods

The biological samples analysed in the present investigation were provided by the Necker and Tenon

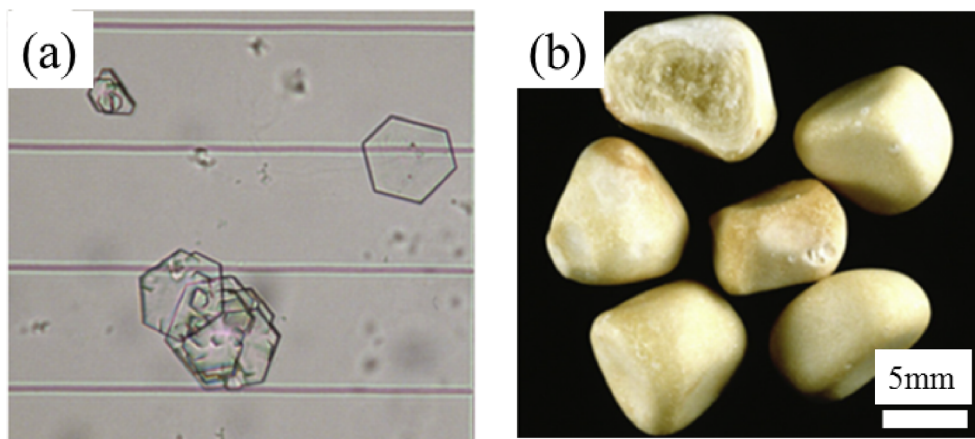


Figure 1. Optical images of (a) cystine crystallites in urine and (b) of cystine kidney stones (from Letavernier *et al.* [19]).

hospitals, following the usual ethics procedures strictly [13]. All participants (adults or parents of children participating in the study) gave their verbal consent, documented by the researchers, for use of the material. Samples were examined without knowledge of the name of the patient or other identifying data. Ethical approval for the study was obtained from the ethics committee of Tenon Hospital. The investigation conformed to the principles of the Declaration of Helsinki.

Regarding cystinuria, SEM observations have been performed on cystine crystals present in urine. This investigation is also based on SEM observations, FTIR and neutron diffraction data on twenty-five cystine kidney stones which has already been published [24] and on the kidney stone data bank in which 1216 kidney stones have been studied through FTIR spectroscopy. Regarding cystinosis, only one kidney biopsy has been considered in this investigation.

For precise characterisation of the surface of an abnormal biological sample, observations at the micrometre scale were performed using a FEI/Philips XL40 environmental scanning electron microscope [39,40]. Compared to a conventional scanning electron microscope this device does not need a conductive coating and thus permits direct observation with no damage to the sample. Imaging was performed with a low accelerating voltage (around 1 kV).

At the micrometre scale, the pathological calcifications were first characterised using FTIR

spectroscopy (Vector 22, Bruker Spectrospin, Wissembourg, France) as previously described [41,42]. Data were collected in absorption mode between 4000 and 400 cm^{-1} , with 4 cm^{-1} spectral resolution.

Chemical characterisations of the pathological calcifications in kidney biopsies at the nanometre scale were performed by two techniques which use mid-infrared photons, namely AFM-IR and OPTIR.

The AFM-IR system used for this study is a NanoIR2 (Bruker Nano, Santa Barbara). It couples an AFM system with a quantum cascade laser focus on the AFM tip for top-down illumination. The laser covers the wavenumber range from 900 cm^{-1} to 1945 cm^{-1} with a tuneable repetition rate which allows enhanced mode acquisition [57] which is more sensitive than the setup we have already used to study abnormal deposits in the kidney [58]. AFM acquisitions were made in contact mode with a gold-coated silicon cantilever (Budget Sensors, contact mode, 13 kHz, 0.2 N/m). For this study, only AFM topographies were acquired and all local IR spectra were collected with 1 cm^{-1} spectral resolution and an average of 20 acquisitions.

OPTIR measurements (spectra and images) were done on a mIRage™ Infrared Microscope (Photothermal Spectroscopy Corp., Santa Barbara, CA, USA). Samples were placed on low-e microscope slides (MirrIR, Kevley Technologies, Tienta Sciences, Indianapolis). To generate data high signal-to-noise ratio, 20–50 spectra were collected in reflection mode, at 2 cm^{-1} spectral data points spac-

ing, through a 40 \times , 0.78 NA, 8 mm working distance Schwarzschild objective. The pump IR source was a pulsed, tunable four-stage QCL device, scanning from 800 to 1900 cm^{-1} , and we used a CW 532 nm visible variable power probe laser.

A Density Functional Theory-Dispersion corrected (DFT-D) IR spectrum was calculated. The computational procedures are similar to those described in our earlier studies [59–63].

3. Results and discussion

3.1. *The case of cystinuria*

The structural characterisation of cystine kidney stones has been discussed in several publications. Consistent with its crystallographic structure (hexagonal crystal system, $P6_122$ space group), all the papers on synthetic [47–54] or biological [18–21,24,55,56,64–66] cystine have reported a hexagonal morphology. On SEM observations, at the micrometre scale, we can clearly see the hexagonal shape of the cystine deposits in kidney stones from mice and humans affected by cystinuria (Figure 2).

For a complete classification of kidney stones [5, 6], the determination of the morphology of these concretions is complemented by chemical composition determined by FTIR spectroscopy [41,42,67]. In Figure 3, we plot the FTIR spectrum of biological cystine (in this case from a human kidney stone). It is compared with a theoretical (DFT-D) spectrum in the IR spectral range from 700 to 1800 cm^{-1} on which the present study focuses.

The IR spectrum of zwitterionic cystine was calculated between 500 and 3500 cm^{-1} . In the experimental IR spectrum (Figure 3, Table 1), the 1035 cm^{-1} absorption peak corresponds to the C–N stretching vibration. The bands at 1372, 1197 and 1125 cm^{-1} are the C–C stretching vibrations, and that at 1406 cm^{-1} is due to CH_2 –CO deformation. Finally, the band at 1490 cm^{-1} is due to COO^- stretching while bands at 1584 and 845 cm^{-1} are due to the asymmetric deformation and rocking vibrations of NH_3^+ , supporting the zwitterionic nature of cystine in the solid state. These results are consistent with previous publications [68–70].

Comparing the experimental with the DFT-D spectrum, a global shift in wavenumbers can be observed. Van der Waals interactions, which are difficult

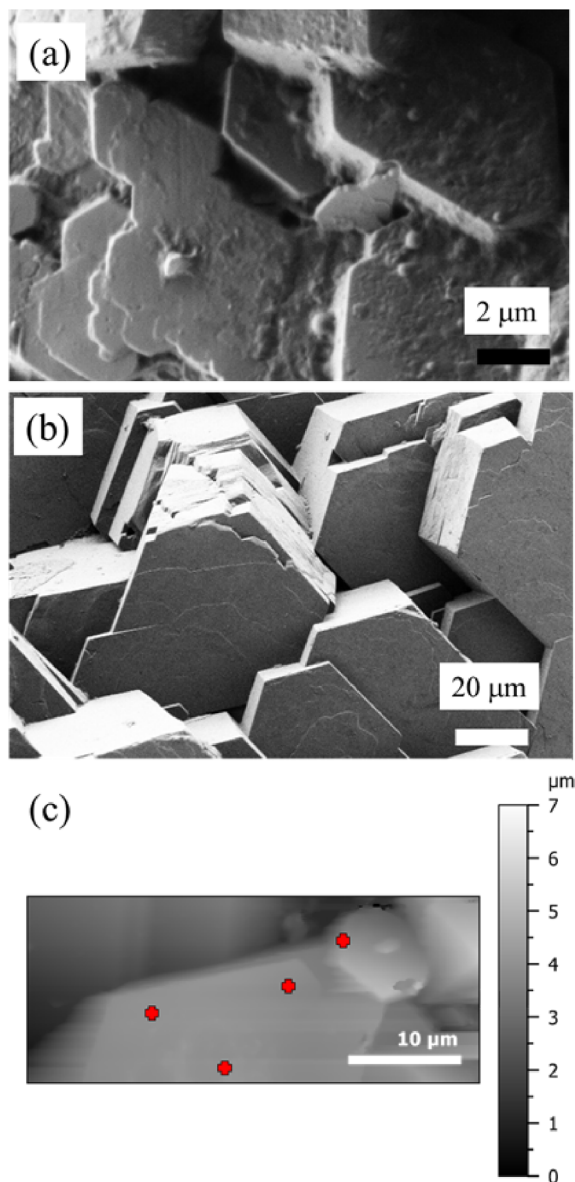


Figure 2. (a) SEM observation of cystine crystallites in kidney stones from mice; cystine crystallites present in human urine (b) by SEM and (c) by AFM. The red crosses on (c) indicate the different points selected for acquisition of IR spectrum using the 50 nm probe.

to evaluate even with the inclusion of the dispersion corrections we used, can explain this well-known discrepancy. Besides, the DFT-D calculations were performed at 0 K whereas the experimental spectrum was recorded at 300 K. Both effects are known to af-

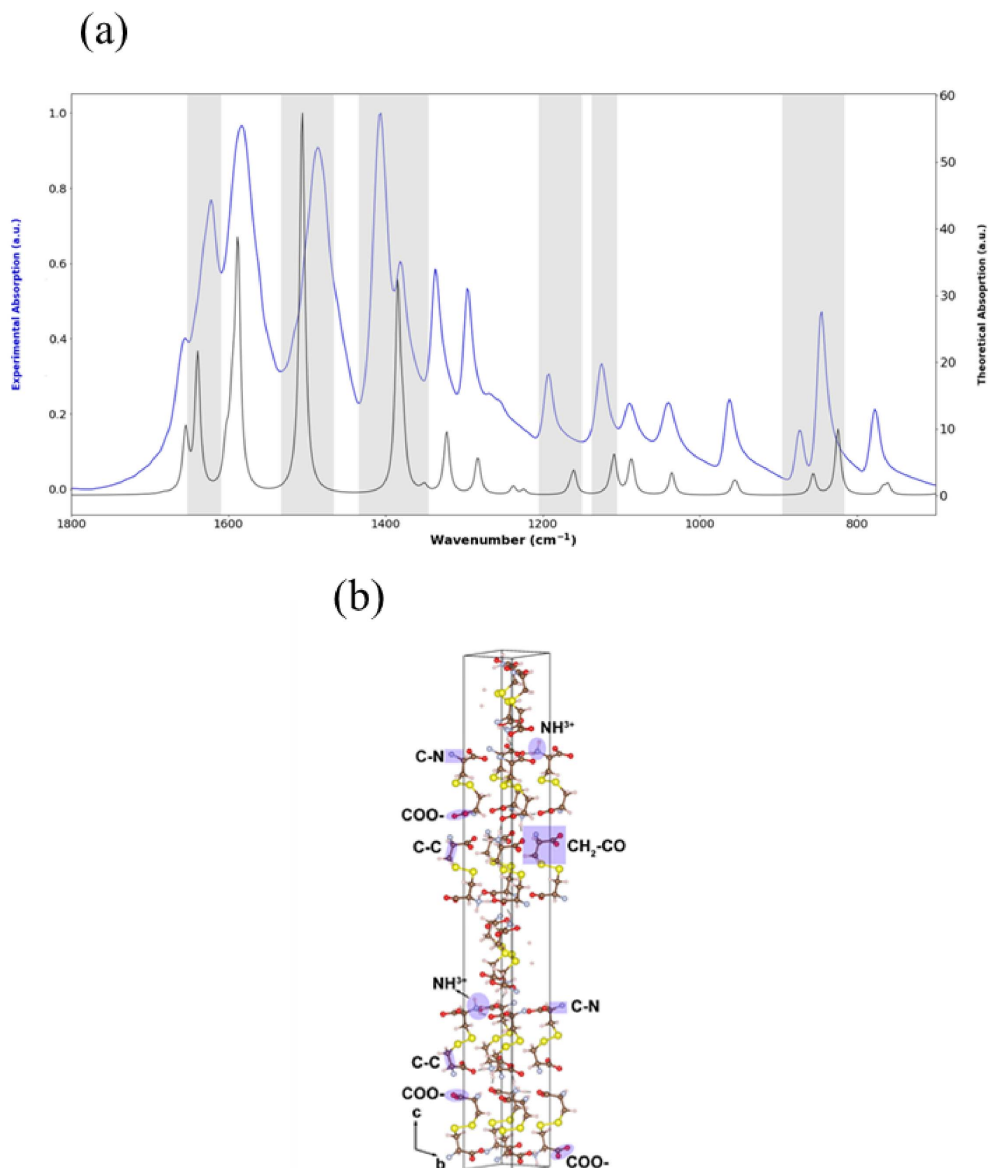


Figure 3. (a) DFT-D theoretical (black) and experimental (blue) IR spectra between 1800 cm^{-1} and 800 cm^{-1} . For the experimental data, a μ FTIR spectrometer was used. The most significant wavenumber shifts between theoretical and experimental absorption bands are highlighted in grey. (b) Crystallographic structure of cystine.

fect the harmonic oscillator approximation negatively. Moreover, the cystine crystal structure is modelled as a periodic defect-free lattice, whereas the experimental sample consists of crystallites of finite sizes; this difference also affects the correspondence between theory and experiment. This small disagreement confirms that the real sample is composed of fi-

nite crystallites that probably contain different types of atomic level crystal defects.

In the human kidney stone case, we have compared the IR spectrum of cystine obtained by μ FTIR and the ones obtained by AFM-IR and OPTIR (Figure 4). Although we can see extensive similarity between all the three spectra, some differences exist.

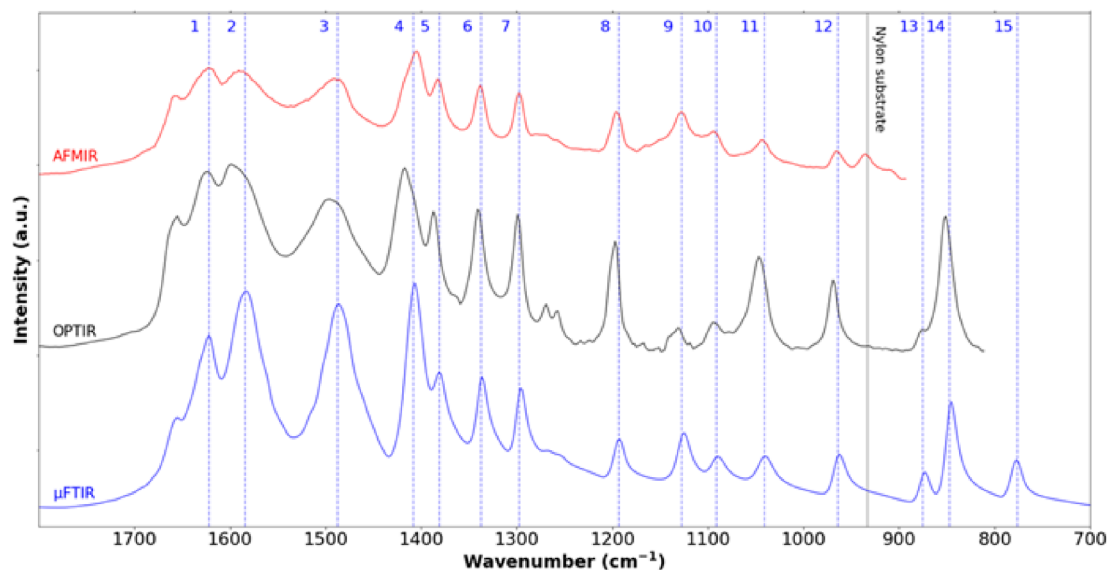


Figure 4. Cystine crystallites in cystinuria. IR spectra collected between 1800 cm^{-1} and 800 cm^{-1} using three different experimental setups namely μ FTIR (blue—cystine kidney stone), OPTIR (black—cystine crystallite in human urine) and AFM-IR (red—cystine crystallite in human urine). We can see the different characteristic IR bands 1622 cm^{-1} (1), 1584 cm^{-1} (2), 1487 cm^{-1} (3), 1408 cm^{-1} (4), 1381 cm^{-1} (5), 1337 cm^{-1} (6), 1297 cm^{-1} (7), 1193 cm^{-1} (8), 1127 cm^{-1} (9), 1091 cm^{-1} (10), 1041 cm^{-1} (11), 964 cm^{-1} (12), 875 cm^{-1} (13), 847 cm^{-1} (14) and 776 cm^{-1} (15). IR absorption band at 933 cm^{-1} corresponds to the nylon support.

Table 1. Infrared bands of cystine and their assignments

1035 cm^{-1}	C–N stretching
$1372, 1197\text{ and }1125\text{ cm}^{-1}$	C–C stretching
1406 cm^{-1}	CH_2 –CO deformation
1490 cm^{-1}	COO^- stretching
$1584\text{ and }845\text{ cm}^{-1}$	NH_3^+ asymmetric deformation and rocking vibrations

We observe a supplementary IR absorption band in the AFM-IR spectrum due to the support material (black vertical line at 933 cm^{-1} in Figure 4). Also, note some small spectral shifts between the spectrum obtained by μ FTIR and those obtained with the two photothermal techniques. These discrepancies seem to be optical in origin but work to understand this fully is still in progress. A point which can already be highlighted is a possible polarisation effect on the observed spectra. Unlike μ FTIR measurement, the light from quantum cascade lasers used in OPTIR and AFM-IR has an intrinsic polarisation which can induce changes in band intensity in spectra of highly

oriented objects such as crystals compared to those from μ FTIR. As a consequence, for each technique it may be possible to have different band intensities from the same sample depending on the orientation of the object. Furthermore, the angle of incident illumination is different from OPTIR and AFM-IR, inducing different polarisation effects even for a sample with the same orientation. AFM-based techniques such as AFM-IR also produces a micrometre scale image of the sample (Figure 2c) which can be compared to SEM observation of the same sample (Figure 2b). This is not the case for OPTIR which is associated with an optical microscope. The red crosses

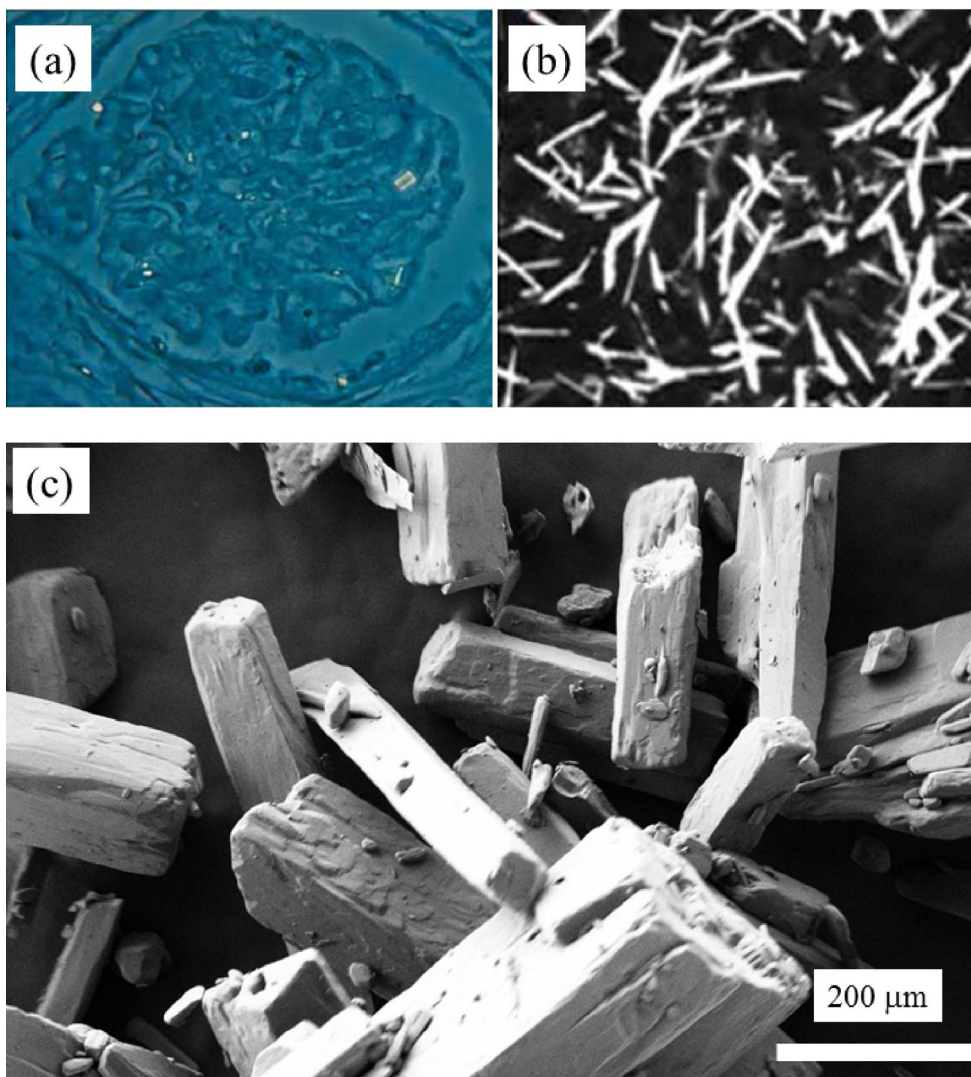


Figure 5. Crystallites in cystinosis. (a) Rectangular morphologies of abnormal deposits observed in kidney (according to [24]). (b) Rectangular morphologies of abnormal deposits observed by slit lamp in the cornea (according to [60]). (c) Synthetic cysteine crystals observed by SEM (Figure 5a from Nesterova *et al.* [29] and Figure 5b from Elmonem *et al.* [71]).

in Figure 2c indicate different points on which the 50 nm probe has been positioned to acquire an IR spectrum.

3.2. The case of cystinosis

3.2.1. Observations of abnormal deposits through optical microscope

The cystinosis situation is quite different from cystinuria. An analysis of the literature [29–31,71,72]

indicates that cystine is the only compound represented in the abnormal deposits and that such crystals (Figures 5 and 6) do not exhibit a hexagonal morphology. Optical microscopy in contrast shows a rectangular crystal morphology in both the kidney (Figure 5a, according to Nesterova *et al.* [29]) and the cornea (Figure 5b, according to Elmonem *et al.* [71]).

A kidney biopsy from a patient (B1742) reveals rectangular crystal morphology in the abnormal deposits (Figure 6). However, such an examination

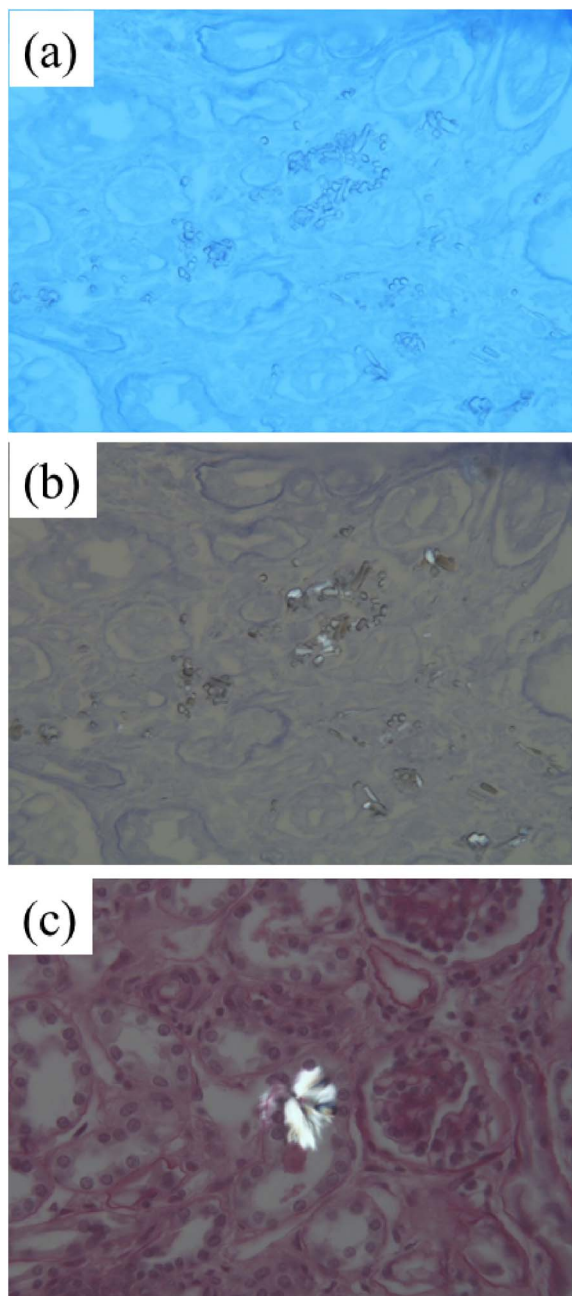


Figure 6. Light microscopy images from the kidney biopsy of a patient with cystinosis. (a) Toluidine Blue ($\times 400$). (b) Small isolated or aggregated crystals. (c) Birefringent aggregated rectangular crystals seen under polarised light.

is not a characterisation of the chemistry of these structures.

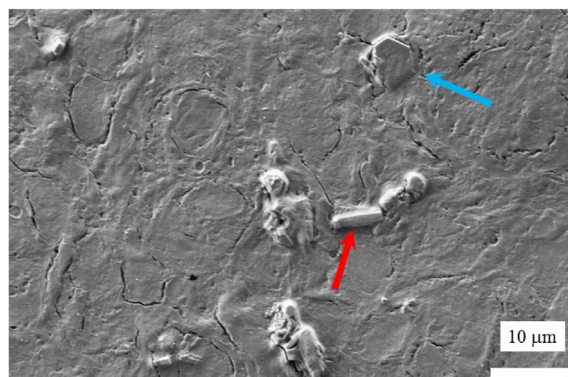


Figure 7. SEM observation of abnormal deposits in the kidney biopsy of a cystinosis patient (kidney biopsy deposited on a low-e microscope slide).

3.2.2. Characterisation at the micrometre scale

We start by locating the abnormal deposits in the kidney biopsy (B1742) by SEM. At the micrometre scale, Figure 7 shows the presence of two kinds of morphologies, the usual cystine hexagonal one (blue arrow), and the morphology typical in a cystinosis patient i.e. a rectangular one (red arrow). Note that with dimensions of 4–5 μm , such hexagonal crystals can be detected by optical microscopy if isolated, but this is difficult if they are embedded in tissue, as in this example.

We then performed a range of μFTIR experiments (Figure 8, Table 2). In the top panel of the figure, we have indicated the IR bands associated with cystine by blue numbers, and in the bottom panel those of cysteine by red. The three IR spectra of the sample (black in Figure 8 corresponding to the abnormal deposits displayed in Figure 7) in fact arise from a combination of IR bands associated with tissue (black lines in Figure 8) and those associated with cystine (blue line in Figure 8). The first three IR bands (1, 2, 3 in blue in Table 2) are obscured by signal from the tissue. This is consistent with the literature on physicochemical characterisation of crystals present in the tissue of patients with cystinosis. We now present results from nanometre scale IR spectroscopy.

3.2.3. Characterisation at the nanometre scale

We chose the same sample for OPTIR experiments as the one we used for μFTIR . Figure 9 shows IR

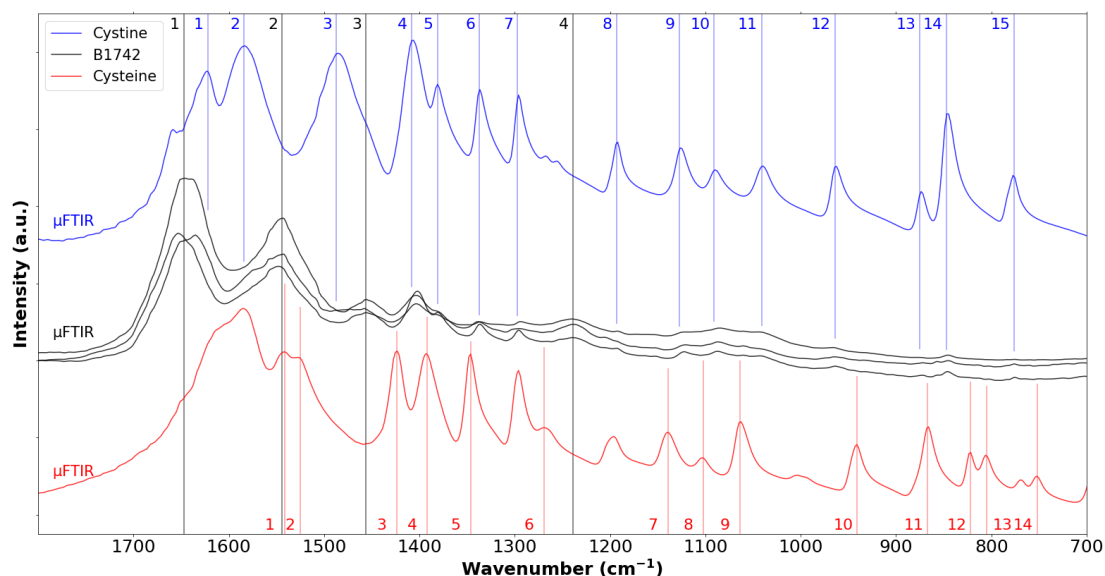


Figure 8. FTIR spectra of the B1742 sample (black) compared to the IR spectra of cystine (blue) and cysteine (red), coloured dashed lines indicate the specific positions for each species, respectively, B1742 sample (black), cystine (blue) and cysteine (red).

spectra from the sample (black spectra) collected by OPTIR with a device yielding a spatial resolution of ≈ 500 nm. This explains why tissue IR bands can still be observed but with lower relative intensity (black lines 1, 2, 3 and 4). This new set of experimental data shows cystine IR bands (Table 2). However the striking point of these OPTIR measurement is the observation of IR peaks related to cysteine at 1541 cm^{-1} (IR band number 1 of cysteine; all subsequent band numbers also correspond to those of cysteine), 1521 cm^{-1} (band 2), 1424 cm^{-1} (band 3 of cysteine), 1392 cm^{-1} (band 4), 1345 cm^{-1} (band 5), 1060 cm^{-1} (band 9) and 867 cm^{-1} (band 11); those at 1060 cm^{-1} (band 9) and 867 cm^{-1} (band 11) are quite intense.

To perform structural and chemical characterisation at the nanometre scale with the AFM-IR experimental setup, part of the kidney biopsy was deposited on a CaF_2 slide. SEM (Figure 10) was performed prior to AFM-IR and led to similar conclusions regarding the morphology of the biopsy crystallites.

Figure 11 plots a localised IR spectrum collected with the ≈ 50 nm spatial resolution AFM-IR experimental setup; the tissue bands are not apparent be-

cause the high spatial resolution confines the IR signal to the crystals in the biopsy only. At first sight, the IR bands of the sample are similar to the IR bands of cystine. Nevertheless, it seems that various shoulders are observed in the AFM-IR spectrum which likely correspond to cysteine (1424 cm^{-1} , band 3; 1392 cm^{-1} , band 4; 1345 cm^{-1} , band 5; 1269 cm^{-1} , band 6; 1137 cm^{-1} , band 7; and 1060 cm^{-1} , band 9).

In conclusion, from the results obtained at the nanoscale with both techniques, OPTIR and AFM-IR, it seems that the sample can be understood as a mixing of cystine and cysteine instead of pure cystine as observed in μFTIR .

3.3. Discussion

As previously reported, cystinosis affects all ocular structures [73]. The most frequently described ocular manifestation is cystine crystal deposition in the cornea [74]. As underlined by Csorba *et al.* [65], *in vivo* confocal microscopy (IVCM) constitutes the best imaging technique to characterise corneal cystine crystals *in vivo* [72–81]. This literature indicates that IVCM enables quantification and identification of the

Table 2. Position of the IR bands obtained for the reference compounds (cystine and cysteine) and for the samples in μ FTIR, OPTIR and AFM-IR

Sample	Reference compounds		Patient		
	Cystine	Cysteine	μ FTIR	OPTIR	AFM-IR
1-1647 cm^{-1}			1	1	
	1-1622 cm^{-1}			1	1
	2-1584 cm^{-1}			2	2
2-1544 cm^{-1}			2	2	
		1-1541 cm^{-1}		1	
		2-1521 cm^{-1}		2	
	3-1487 cm^{-1}				3
3-1456 cm^{-1}			3	3	
		3-1424 cm^{-1}		3	3
	4-1408 cm^{-1}		4	4	4
		4-1392 cm^{-1}		4	
	5-1381 cm^{-1}		5	5	5
		5-1345 cm^{-1}		5	5
	6-1337 cm^{-1}		6	6	6
	7-1297 cm^{-1}		7	7	7
		6-1269 cm^{-1}			6
4-1239 cm^{-1}			4	4	
	8-1193 cm^{-1}		8	8	8
		7-1137 cm^{-1}			7
	9-1127 cm^{-1}		9	9	9
		8-1101 cm^{-1}			
	10-1091 cm^{-1}		10	10	10
		9-1060 cm^{-1}		9	9
	11-1041 cm^{-1}		11	11	11
	12-964 cm^{-1}		12	12	12
		10-937 cm^{-1}			
	13-875 cm^{-1}		13		
	14-847 cm^{-1}		14		
		11-867 cm^{-1}		11	
		12-817 cm^{-1}			
		13-805 cm^{-1}			
	15-776 cm^{-1}		15		
		14-750 cm^{-1}			

deposits at the cellular level, and is thus considered as the gold standard for ophthalmological follow-up of patients with cystinosis [73–81]. Nevertheless, it is worth mentioning that a detailed description of crys-

tal morphology is not equivalent to chemical identification.

The physicochemistry of cystinosis seems to be quite inconsistent. The literature clearly indicates the

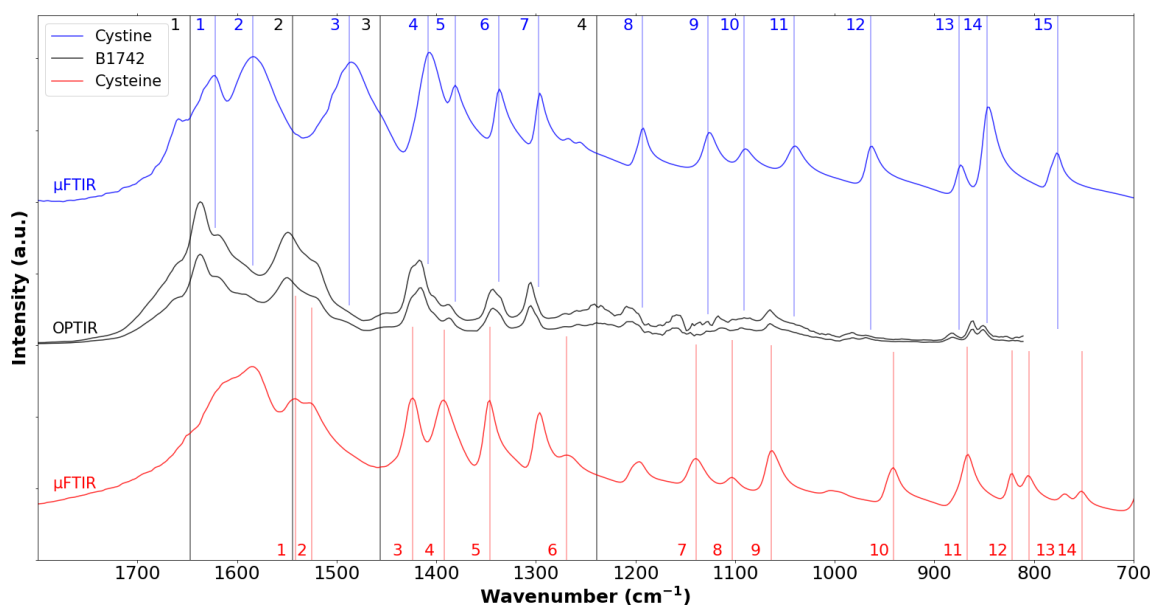


Figure 9. OPTIR spectra of the B1742 sample (black line) compared to the IR spectra of cystine (blue) and cysteine (red).

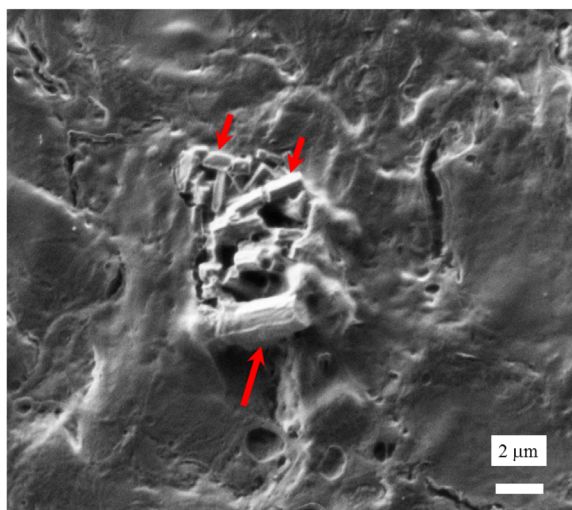


Figure 10. SEM observation of abnormal deposits (red arrows) in the kidney biopsy of a nephropathic cystinosis patient.

presence of rectangular crystals made of cystine [29–31,71–79,81]. Such morphology is not expected for cystine crystals which are typically hexagonal for synthetic [47–54] as well as for biological [18–21,24,55,56,

64–66] samples. Rectangular-like crystallites are observed in the case of synthetic cysteine (Figure 5c). This observation is complemented by our IR data collected at the nanometre scale using OPTIR (Figure 9) and AFM-IR (Figure 11) which clearly suggest the presence of domains of cysteine and of cystine. Such chemical heterogeneity may explain why the signals measured by AFM-IR and OPTIR are not exactly the same. In our study, we have also identified the presence of hexagonal crystals (Figure 7). Such mixing is consistent with the chemistry of these two compounds, namely that cysteine is spontaneously oxidised to cystine at neutral pH [82–84]. All these data seem to show that in fact cystinosis is linked to the pathogenesis of cysteine crystallites associated with a rectangular morphology, and to the pathogenesis of cystine, as evidenced by our observation of hexagonal cystine crystals.

It is worth pointing out that there is an analogous crystalline conversion which occurs in kidney stones, from weddellite (unstable) to whewellite (stable). In this case, the conversion also results in contradictory FTIR spectra indicating whewellite whereas bipyramidal crystallites, a morphology specific to weddellite, can be observed [85]. In fact, the

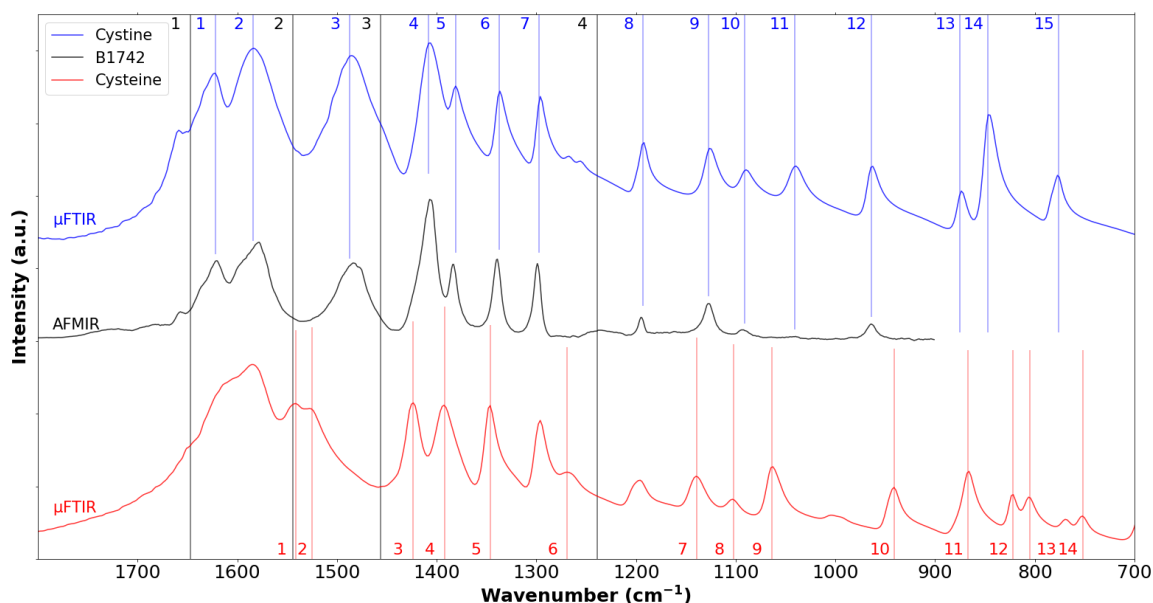


Figure 11. AFM-IR spectrum of the B1742 sample (black line) compared to the IR spectra of cystine (blue line) and cysteine (red line).

IR spectra corresponding to such kidney stones (undergoing the weddellite to whewellite phase transition) exhibit IR spectra which do not correspond exactly to whewellite. Some subtle differences exist which indicate the presence of amorphous calcium oxalate monohydrate which constitutes an intermediate state reflecting the dissolution–recrystallisation process. In our case it seems that a phase transition also occurs but probably without a dissolution–recrystallisation process and thus a similar situation is observed i.e. a lack of intensity for the IR band at 1584 cm^{-1} . It may be due to the fact that the final chemical composition comprising cystine and cysteine associated with acicular crystallites may alter the intensity of IR bands. Work is in progress to better understand this experimental observation.

Finally, we have to mention a possible weak point of this investigation which is related to the low number of samples considered in this investigation. Although the section of this study dedicated to cystinuria is based on a large number of publications, only one patient has been considered in this research. Despite this fact, we believe that the existence of crystallites of pure cystine as well as the well-known phase

transition between cysteine and cystine constitute strong arguments supporting the idea that cystinosis leads to pathogenic cysteine crystallites.

4. Conclusion

A comprehensive set of SEM micrometre scale and IR micrometre and nanometre scale data suggests that cystinosis is related to the pathogenesis of rectangular crystals of cysteine and not cystine. This is probably due to the well-known phase transition between cysteine and cystine which occurs at room temperature.

Acknowledgements

Computational resources and services were also provided by the Shared ICT Services Centre funded by the Vrije Universiteit Brussel, the Flemish Supercomputer Center (VSC) and FWO. FT wishes to acknowledge the VUB for support, including a Strategic Research Program awarded to his group.

References

- [1] J. A. Sayer, *Nephron Exp. Nephrol.*, 2008, **110**, e37-e43.
- [2] L. Beara-Lasic, V. O. Edvardsson, R. Palsson, J. C. Lieske, D. S. Goldfarb, D. S. Milliner, *Clin. Rev. Bone Miner. Metab.*, 2012, **10**, 2-18.
- [3] P. M. Ferraro, A. D'Addessi, G. Gambaro, *Nephrol. Dial. Transplant.*, 2013, **28**, 811-820.
- [4] G. Rumsby, *Int. J. Surg.*, 2016, **36**, 590-595.
- [5] M. Daudon, C. A. Bader, P. Jungers, *Scanning Microsc.*, 1993, **7**, 1081-1104.
- [6] M. Daudon, A. Dessombz, V. Frochot, E. Letavernier, J. P. Haymann, P. Jungers, D. Bazin, *C. R. Chim.*, 2016, **19**, 1470-1491.
- [7] P. Cochat, *Kidney Int.*, 1999, **55**, 2533-2547.
- [8] E. Leumann, B. Hoppe, *J. Am. Soc. Nephrol.*, 2001, **12**, 1986-1993.
- [9] M. Daudon, P. Junger, D. Bazin, *N. Engl. J. Med.*, 2008, **359**, 100-102.
- [10] M. Daudon, D. Bazin, G. André, P. Jungers, A. Cousson, P. Chevallier, E. Véron, G. Matzen, *J. Appl. Cryst.*, 2009, **42**, 109-115.
- [11] G. Bollée, C. Dollinger, L. Boutaud, D. Guillemot, A. Bensman, J. Harambat, P. Deteix, M. Daudon, B. Knebelmann, I. Ceballos-Picot, *J. Am. Soc. Nephrol.*, 2010, **21**, 679-688.
- [12] G. Bollée, J. Harambat, A. Bensman, B. Knebelmann, M. Daudon, I. Ceballos-Picot, *Clin. J. Am. Soc. Nephrol.*, 2012, **7**, 1521-1527.
- [13] A. Dessombz, D. Bazin, P. Dumas, C. Sandt, J. Sule-Suso, M. Daudon, *PLoS One*, 2011, **6**, article no. e28007.
- [14] D. Bazin, M. Daudon, *Ann. Biol. Clin.*, 2015, **73**, 517-534.
- [15] P. Eriksson, T. Denneberg, H. G. Tiselius, *Urol. Res.*, 1996, **24**, 39-43.
- [16] A. Dessombz, E. Letavernier, J.-P. Haymann, D. Bazin, M. Daudon, *J. Urol.*, 2015, **193**, 1564-1569.
- [17] E. Pras, N. Arber, I. Aksentijevich, G. Katz, J. M. Schapiro, L. Prosen, L. Gruberg, D. Harel, U. Liberman, J. Weissenbach, M. Pras, D. L. Kastner, *Nat. Genet.*, 1994, **6**, 415-419.
- [18] H. Bouzidi, M. Daudon, *Ann. Biol. Clin.*, 2007, **65**, 473-481.
- [19] E. Letavernier, O. Traxer, J.-P. Haymann, D. Bazin, M. Daudon, *Prog. Urol. – FMC*, 2012, **22**, F119-F123.
- [20] J. P. Haymann, M. Livrozet, J. Rode, S. Doizi, O. Traxer, V. Frochot, E. Letavernier, D. Bazin, M. Daudon, *Prog. Urol. – FMC*, 2021, **31**, F1-F7.
- [21] M. Livrozet, S. Vandermeersch, L. Mesnard, E. Thioulouse, J. Jaubert, J.-J. Boffa, J.-P. Haymann, L. Baud, D. Bazin, M. Daudon, E. Letavernier, *PLoS One*, 2014, **9**, article no. e102700.
- [22] M. Daudon, F. Cohen-Solal, F. Barbey, M.-F. Gagnadoux, B. Knebelmann, P. Jungers, *Urol. Res.*, 2003, **31**, 207-211.
- [23] A. P. Evan, F. L. Coe, J. E. Lingeman, Y. Shao, B. R. Matlaga, S. C. Kim, S. B. Bledsoe, A. J. Sommer, M. Grynepas, C. L. Phillips, E. M. Worcester, *Kidney Int.*, 2006, **69**, 2227-2235.
- [24] D. Bazin, M. Daudon, G. André, R. Weil, E. Véron, G. Matzen, *J. Appl. Cryst.*, 2014, **47**, 719-725.
- [25] K. H. Andreassen, K. V. Pedersen, S. S. Osther, H. U. Jung, S. K. Lilda, P. J. S. Osther, *Urolithiasis*, 2016, **44**, 65-76.
- [26] W. A. Gahl, J. G. Thoene, J. A. Schneider, *N. Engl. J. Med.*, 2002, **347**, 111-121.
- [27] A. Jamalpoor, C. AGH van Gelder, F. A. Yousef Yengej, E. A. Zaal, S. P. Berlingerio, K. R. Veys, C. P. Casellas, K. Voskuil, K. Essa, C. M. E. Ammerlaan, L. R. Rega, R. van der Welle, M. R. Lilien, M. B. Rookmaaker, H. Clevers, J. Klumperman, E. Levchenko, C. R. Berkers, M. C. Verhaar, M. Altelaar, R. Masereeuw, M. J. Janssen, *EMBO Mol. Med.*, 2021, **13**, article no. e13067.
- [28] A. Servais, C. Goizet, A. Bertholet-Thomas, S. Decramer, B. Llanas, G. Choukroun, R. Novo, *Néphrol. Thérapeut.*, 2015, **11**, 152-159.
- [29] G. Nesterova, W. Gahl, *Pediatr. Nephrol.*, 2008, **23**, 863-878.
- [30] P. D. Frazier, V. G. Wong, *Arch. Ophthalmol.*, 1968, **80**, 87-91.
- [31] J. A. Centeno, K. G. Ishak, F. G. Mullick, W. A. Gahl, T. J. O'Leary, *Appl. Spectrosc.*, 1994, **48**, 569-572.
- [32] S. Dahaoui, V. Pichon-Pesme, J. A. K. Howard, C. Lecomte, *J. Phys. Chem. A*, 1999, **103**, 6240-6250.
- [33] D. Bazin, M. Daudon, C. Combes, C. Rey, *Chem. Rev.*, 2012, **112**, 5092-5120.
- [34] D. Bazin, M. Daudon, *J. Phys. D: Appl. Phys.*, 2012, **45**, article no. 383001.
- [35] D. Bazin, J.-P. Haymann, E. Letavernier, J. Rode, M. Daudon, *Presse Med.*, 2014, **43**, 135-148.
- [36] D. Bazin, E. Letavernier, J.-P. Haymann, P. Méria, M. Daudon, *Prog. Urol.*, 2016, **26**, 608-618.
- [37] E. Tsolaki, S. Bertazzo, *Materials*, 2019, **12**, article no. 3126.
- [38] N. Vidavsky, J. A. M. R. Kunitake, L. A. Estroff, *Adv. Healthc. Mater.*, 2020, article no. e2001271.
- [39] F. Brisset, M. Repoux, J. Ruste, F. Grillon, F. Robaut, *Microscopie Électronique à Balayage et Microanalyses*, EDP Sciences, Les Ulis, France, 2009.
- [40] R. F. Egerton, *Physical Principles of Electron Microscopy, An Introduction to TEM, SEM, and AEM*, Springer-Verlag, US, 2005.
- [41] N. Quy Dao, M. Daudon, *Infrared and Raman Spectra of Calculi*, Elsevier, Paris, 1997.
- [42] L. Estepa, M. Daudon, *Biospectroscopy*, 1997, **3**, 347-369.
- [43] A. Dazzi, F. Glotin, R. Carminati, *J. Appl. Phys.*, 2010, **107**, article no. 124519.
- [44] A. Dazzi, C. B. Prater, *Chem. Rev.*, 2017, **117**, 5146-5173.
- [45] D. Zhang, C. Li, C. Zhang, M. N. Slipchenko, G. Eakins, J.-X. Cheng, *Sci. Adv.*, 2016, **2**, article no. e1600521.
- [46] O. Klementieva, C. Sandt, I. Martinsson, M. Kansiz, G. K. Gouras, F. Borondics, *Adv. Sci.*, 2020, **7**, article no. 1903004.
- [47] M. Ejgenberg, Y. Mastai, *Cryst. Growth Des.*, 2012, **12**, 4995-5001.
- [48] L. N. Poloni, Z. Zhu, N. Garcia-Vázquez, A. C. Yu, D. M. Connors, L. Hu, A. Sahota, M. D. Ward, A. G. Shtukenberg, *Cryst. Growth Des.*, 2017, **17**, 2767-2781.
- [49] J. D. Rimer, Z. An, Z. Zhu, M. H. Lee, D. S. Goldfarb, J. Wesson, M. D. Ward, *Science*, 2010, **330**, 337-341.
- [50] D. Heimbach, D. Jacobs, S. C. Müller, A. Hesse, *Urology*, 2000, **55**, 17-21.
- [51] T. Mandal, A. G. Shtukenberg, A. C. Yu, X. Zhong, M. D. Ward, *Cryst. Growth Des.*, 2016, **16**, 423-431.
- [52] M. Adobes-Vidal, A. G. Shtukenberg, M. D. Ward, P. R. Unwin, *Cryst. Growth Des.*, 2017, **17**, 1766-1774.
- [53] M. Song, W. Li, X. Zhang, J. Liu, K. Li, H. Zhang, *ACS Earth Space Chem.*, 2021, **5**, 1525-1534.
- [54] A. G. Shtukenberg, L. N. Poloni, Z. Zhu, Z. An, M. Bhandari, P. Song, A. L. Rohl, B. Kahr, M. D. Ward, *Cryst. Growth Des.*, 2015, **15**, 921-934.

- [55] G. H. Noehden, *Ann. Philos.*, 1824, **7**, article no. 146.
- [56] S. R. Khan, R. L. Hackettm, *J. Urol.*, 1986, **135**, 818-825.
- [57] F. Lu, M. Belkin, *Opt. Express*, 2011, **19**, 19942-19947.
- [58] E. Esteve, Y. Luque, J. Waeytens, D. Bazin, L. Mesnard, C. Jouanneau, P. Ronco, A. Dazzi, M. Daudon, A. Deniset-Besseau, *Anal. Chem.*, 2020, **92**, 7388-7392.
- [59] J. Vekeman, F. Tielens, *Nanomaterials*, 2020, **10**, article no. 540.
- [60] I. Petit, G. D. Belletti, T. Debroise, M. Llansola, I. T. Lucas, C. Leroy, C. Bonhomme, L. Bonhomme-Coury, D. Bazin, M. Daudon, E. Letavernier, J. P. Haymann, V. Frochot, F. Babonneau, P. Quaino, F. Tielens, *Chem. Select.*, 2018, **3**, 8801-8812.
- [61] T. Debroise, E. Colombo, G. Belletti, J. Vekeman, Y. Su, R. Papoular, N. S. Hwang, D. Bazin, M. Daudon, P. Quaino, F. Tielens, *Cryst. Growth Des.*, 2020, **20**, 2553-2561.
- [62] I. Can Oğuz, H. Guesmi, D. Bazin, F. Tielens, *J. Phys. Chem. C*, 2019, **123**, 20314-20318.
- [63] F. Tielens, J. Vekeman, D. Bazin, M. Daudon, *C. R. Chim.*, 2022, **25**, no. S1, 209-218.
- [64] A. Hesse, G. Sanders, D. B. Leusman, *Scan. Electron. Microsc.*, 1986, **1986**, 1705-1712.
- [65] M. Racek, J. Racek, I. Hupáková, *Scand. J. Clin. Lab. Investig.*, 2019, **79**, 208-217.
- [66] T. Qiao, R.-H. Ma, X.-B. Luo, Y.-Y. Feng, X.-Q. Wang, P.-M. Zheng, Z.-L. Luo, *Eur. J. Med. Res.*, 2012, **17**, article no. 6.
- [67] M. Daudon, D. Bazin, *C. R. Chim.*, 2016, **19**, 1416-1423.
- [68] S. K. Chandran, R. Paulraj, P. Ramasamy, *Spectrochim. Acta A: Mol. Biomol. Spectr.*, 2015, **151**, 432-437.
- [69] T. U. Devi, N. Lawrence, R. Rameshbabu, S. Selvanayagam, H. Stoeckli-Evans, G. Bhagavannarayana, K. Ramamurthi, *J. Miner. Mater. Charact. Eng.*, 2010, **9**, 495-507.
- [70] Y. Su, E. P. Hessou, P. Quiano, E. Colombo, A. Moussadik, I. Lucas, V. Frochot, M. Daudon, D. Bazin, F. Tielens, submitted, to be published in the *Journal of Crystal Growth*.
- [71] M. A. Elmonem, K. R. Veys, N. A. Soliman, M. van Dyck, L. P. van den Heuvel, E. Levchenko, *Orphanet J. Rare Dis.*, 2016, **11**, article no. 47.
- [72] H. Liang, C. Baudouin, R. T. J. Hassani, F. Brignole-Baudouin, A. Labbe, *Investig. Ophthalmol. Vis. Sci.*, 2015, **56**, 3218-3225.
- [73] A. Csorba, E. Maka, O. A. Maneschg, A. Szabó, N. Szentmáry, M. Csidey, M. Resch, L. Imre, K. Knézy, Z. Z. Nagy, *BMC Ophthalmol.*, 2020, **20**, article no. 73.
- [74] H. Liang, C. Baudouin, R. Tahiri Joutei Hassani, F. Brignole-Baudouin, A. Labbe, *Investig. Ophthalmol. Vis. Sci.*, 2015, **56**, 3218-3225.
- [75] A. H. Alsuhaibani, A. O. Khan, M. D. Wagoner, *Br. J. Ophthalmol.*, 2005, **89**, 1530-1531.
- [76] F. Shams, I. Livingstone, D. Oladiwura, K. Ramaesh, *Clin. Ophthalmol.*, 2014, **8**, 2077-2084.
- [77] A. Labbe, P. Niaudet, C. Loirat, M. Charbit, G. Guest, C. Baudouin, *Ophthalmology*, 2009, **116**, 870-876.
- [78] C. N. Grupcheva, S. E. Ormonde, C. McGhee, *Arch Ophthalmol.*, 2002, **120**, 1742-1745.
- [79] A. M. Pinxten, M. T. Hua, J. Simpson, K. Hohenfellner, E. Levchenko, I. Casteels, *Ophthalmol. Ther.*, 2017, **6**, 93-104.
- [80] H. Liang, A. Labbe, J. Le Mouhaer, C. Plisson, C. Baudouin, *Investig. Ophthalmol. Vis. Sci.*, 2017, **58**, 2275-2283.
- [81] A. Labbe, C. Baudouin, G. Deschenes, C. Loirat, M. Charbit, G. Guest, P. Niaudet, *Mol. Genet. Metab.*, 2014, **111**, 314-320.
- [82] O. Warburg, *Biochem. Z.*, 1927, **187**, article no. 255.
- [83] L. H. Gray, *Progress in Radiobiology*, vol. 267, Oliver and Boyd, Ltd, Edinburgh, UK, 1956.
- [84] D. L. Dewey, J. Beecher, *Nature*, 1965, **206**, 1369-1370.
- [85] D. Bazin, C. Leroy, F. Tielens, C. Bonhomme, L. Bonhomme-Coury, F. Damay, D. Le Denmat, J. Sadoine, J. Rode, V. Frochot, E. Letavernier, J.-P. Haymann, M. Daudon, *C. R. Chim.*, 2016, **19**, 1492-1503.